photonics

MDPI

Article

Wavelength-Dependent Calcium Signaling Response to Photobiomodulation in Pancreatic Cells

Kelli Fowlds [1], Anne M. Alsup [1], Abhidha Kunwar [1], Carly M. Darden [2], Jacob M. Luber [3], Michael C. Lawrence [4] and Michael Cho [1,*]

[1] Department of Bioengineering, The University of Texas at Arlington, Arlington, TX 76010, USA; kelli.fowlds@mavs.uta.edu (K.F.); anne.alsup@mavs.uta.edu (A.M.A.); axk5162@mavs.uta.edu (A.K.)
[2] Simmons Transplant Institute, Baylor Scott & White Health, Dallas, TX 76104, USA; carly.darden@bswhealth.org
[3] Department of Computer Science & Engineering, The University of Texas at Arlington, Arlington, TX 76010, USA; jacob.luber@uta.edu
[4] Islet Cell Laboratory, Baylor Scott and White Research Institute, Dallas, TX 75204, USA; michael.lawrence@bswhealth.org
* Correspondence: michael.cho@uta.edu

Abstract: Diabetes mellitus is a metabolic disorder that is rapidly growing across the world. Our laboratory has recently demonstrated that photobiomodulation (PBM) can couple to its metabolic pathways by modulating calcium dynamics in islet cells, including α- and β-cells. Using computer vision algorithms, changes in PBM-induced calcium dynamics can be verified, and, more importantly, this led us to propose hypotheses that will likely advance our understanding of photostimulatory effects in islet cells. In our previous paper, we determined changes in calcium spiking in response to PBM at 810 nm by manually segmenting the cells and the calcium spiking patterns. We have since developed a computer vison pipeline to automate cell segmentation and subsequent image analyses. By using automated methods for segmentation, registration, tracking, and statistical analysis, we were able to improve the accuracy of previously observed changes in calcium spiking in response to PBM in both cell types. Moreover, this pipeline was applied to elucidate the wavelength-dependent modulation of calcium dynamics at 1064 nm. The extent of increase in calcium spiking appears to have been overestimated by manual analysis, and the machine learning pipeline was able to capture and segment nearly 3-fold more cells, suggesting improved accuracy in the analysis of calcium spiking in islet cells. Detailed calcium analysis also indicates a biphasic dose response among α- and β-cells in response to PBM therapy at different wavelengths. The current findings offer a novel hypothesis and may facilitate the use of translational PBM as a potential therapy for diabetes mellitus.

Keywords: calcium spiking; computer vision algorithms; image analysis; islet cells; photobiomodulation

Received: 17 December 2024
Revised: 13 January 2025
Accepted: 21 January 2025
Published: 23 January 2025

Citation: Fowlds, K.; Alsup, A.M.; Kunwar, A.; Darden, C.M.; Luber, J.M.; Lawrence, M.C.; Cho, M. Wavelength-Dependent Calcium Signaling Response to Photobiomodulation in Pancreatic Cells. *Photonics* **2025**, *12*, 99. https://doi.org/10.3390/photonics12020099

1. Introduction

Photobiomodulation (PBM), also known in the past as low-level laser (light) therapy, uses red or near-infrared (NIR) light to stimulate metabolic interactions, including increased mitochondrial activity. It has been repeatedly demonstrated that the red or NIR light is absorbed by the cytochrome c oxidase (CCO) enzyme [1–3]. The photodissociation of nitric oxide from the enzyme facilitates an influx of oxygen and increases the rate of adenosine triphosphate (ATP) synthesis [4], producing numerous physiological benefits.

1.1. Photobiomodulation Therapy

PBM has become a therapy of interest for a multitude of fields, including wound healing [5–7], inflammation [8], Alzheimer's disease [9,10], stroke [11,12], and traumatic brain injury [13]. Several dermatological procedures have incorporated PBM as a treatment method as well [14]. In the realm of cosmetics, PBM is believed to increase skin strength and hydration and to improve its overall texture [15]. Various forms of light therapy have been used for skin rejuvenation and wrinkle treatments, acne reduction, and fat loss [14,16]. Furthermore, PBM was found to decrease lipid accumulation in adipose-derived stem cells [17], providing potentially significant insights for insulin resistance studies [18]. In addition, numerous studies have investigated the potential benefits of PBM therapy for diabetic patients. Treatments have been shown to improve glucose metabolism [3,19,20] and facilitate diabetic wound healing [21–23].

As red and NIR photons are accepted by the heme subunit of CCO, the mitochondrial membrane potential is increased [21]. Enhanced ATP synthesis has been shown to promote wound healing by accelerating cell proliferation and migration [21]. However, the effectiveness of PBM is dependent on multiple factors, including the wavelength, irradiance, mode (e.g., continuous or pulsed), and exposure rate [21]. Treatment is likely wavelength-dependent, as CCO absorption peaks at approximately 800 nm and diminishes at increasing wavelengths [24–27]. Thus, shorter wavelengths have a more direct effect on CCO and are often used for surface-level therapies (e.g., skin), while longer wavelengths allow for deeper penetration and affect the tissues below the skin or skull in the brain [17,18,21]. Moreover, reviews of multiple studies have found positive effects using both continuous- and pulsed-laser treatments in diabetic would healing models [21,22]. The variation in wavelengths, mode, and fluence (J/cm^2) used in diabetes research is widespread, and thus the optimization of these therapies remains elusive [21].

1.2. Non-Invasive Stimulation of Pancreatic Cells

There are many intricate factors that affect the mechanisms of diabetes and the regulation of glucose levels. Glycogen muscle concentration [3], insulin and glucose tolerance [20], and adipocyte area [19,28] should all be considered when evaluating treatment results from diabetic models. Changes in calcium levels serve as another important indicator for better understanding how pancreatic cells regulate glucose levels. For example, membrane depolarization derived from the closure of ATP-sensitive potassium channels (K_{ATP}) stimulates the opening of voltage-gated Ca^{2+} channels (VGCCs) and induces insulin secretion [29–31]. Our laboratory has previously shown that the frequency and intensity of calcium spiking can be increased through non-invasive stimulatory techniques. Electric field stimulation (EFS) in the physiological range of field strength <2 V/cm was demonstrated to activate VGCCs, increase the calcium spiking frequency, and, subsequently, increase insulin secretion [32]. Interestingly, stimulatory techniques using PBM also showed a significant increase in calcium activity for α- and β-cells [33], but PBM is not expected to couple directly to VGCCs. The analysis of the PBM-induced increase in calcium spiking found it to be correlated with a higher level of insulin secretion. However, a laborious and manual method was used to hand-segment individual cells, which required tens of hours for analyzing just one set of experiments. Furthermore, in the manipulation of the fluorescence intensities that represented the intracellular calcium concentration, it was questioned whether human biases played a role in concluding that this was a potential non-invasive and non-biologic treatment for diabetes mellitus. It is believed that implementing machine learning techniques could significantly accelerate the standardization of PBM parameters through the utilization of more sophisticated models, enabling faster and more comprehensive data analysis [21].

1.3. Complications with Manual Segmentation

Much of the data from these previous experiments have unfortunately been hampered by the limitations of manual analysis techniques. Advancements in technology have led to the quantification of biological images as standard practice in conjunction with examining visual elements, and open source software is increasingly utilized to meet these research needs [34]. However, these programs regularly lack the capacity to perform accurate segmentation to the same extent as modern neural networks. Manual segmentation is a time-consuming process and frequently requires multiple researchers to minimize any potential bias [35]. It is difficult to achieve the complete, accurate segmentation of all cells, and the information obtained from each image is likely limited.

Although traditional programs have previously been demonstrated to be useful tools, advancements in computer vision and machine learning could lead to more sophisticated analyses. These new methods enable investigators to not only perform detailed experiments but also to explore and formulate more intricate hypotheses. While machine learning algorithms often face similar challenges with segmentation, especially on cells with unique shapes, training models with large datasets and providing appropriate parameters can improve accuracy. Automated segmentation techniques are notably faster than manual analysis and can also process far greater amounts of data and provide more detailed results, including spatial and temporal information. We therefore developed and applied a computer vision pipeline, BetaBuddy [36], to previous datasets in order to reassess results determined using hand segmentation methods.

1.4. Study Rationale

Our first application of BetaBuddy was to reanalyze calcium spiking patterns in β-cells that were stimulated by EFS [32]. Automated cell segmentation and analysis confirmed the originally published results but found subtle differences in that the overall calcium spiking activity had been underestimated using manual analysis. In this current study, we applied BetaBuddy and reanalyzed the calcium fluorescence images of mouse islet cells treated with PBM therapy.

The primary objective was to validate the results of the original experiments and assess the differences in the calculated calcium activity between manual and automated segmentation. This study also aimed to assess the efficacy of using a computational model to acquire more specialized data on the effects of photostimulatory treatments and determine whether these algorithms can be employed to optimize cell-type-dependent parameters. To achieve this objective, similar experiments should be conducted using varying wavelengths and exposure durations while maintaining the same fluence.

Interestingly, the automated image analysis indicates that the manual analysis overestimated the extent of calcium spiking in response to PBM. The wavelength dependence of PBM effects was experimentally measured, and the same pipeline was applied to better analyze the data and elucidate the intricate interplay between the two major islet cell types that are believed to counteract one another to regulate glucose homeostasis. We now have the capability to further explore the complicated β-cell physiology due to having access to more accurate and rapid analysis without human biases.

2. Materials and Methods

2.1. Dataset

Mouse-derived βTC6 insulinoma cells (ATCC CRL-3605, Manassas, VA, USA) were cultured in high-glucose DMEM (4.5 g/L, Sigma, Milwaukee, WI, USA), 15% Fetal Bovine Serum (FBS, ThermoFisher, Frederick, MD, USA) and 1% Penicillin–Streptomycin (P-S, 10,000 U/mL, ThermoFisher, Greencastle, PA, USA). Additionally, αTC1 cells (a gift from

the Baylor Scott & White Research Institute) were cultured in low-glucose DMEM (1 g/L, Sigma, Milwaukee, WI, USA), supplemented with 10% FBS and 1% P-S. Both lines were incubated at 37 °C and 5% CO_2.

2.2. Laser Parameters

Of the different NIR wavelengths involved in many PBM studies, 810 nm and 1064 nm are commonly used [24,26]. The absorption of CCO peaks at around 800 nm, and it is theorized that light scattering at 1064 nm can result in deeper penetration [24]. Thus, these wavelengths were chosen for this study. In an effort to further optimize the experimental conditions, multiple levels of irradiance (W/cm^2) and dosing rates (s) were used. These can be precisely controlled in each laser system. Because both lasers have a fixed beam size, the power (W) and rate of delivery were easily manipulated while maintaining a standard fluence (J/cm^2).

For the photostimulation treatments, cells were exposed to a continuous-wave NIR laser of either 810 nm (Cytonsys; Austin, TX, USA) or 1064 nm (Cell Gen Therapeutics, Dallas, TX, USA; model CG-5000) at a 9 J/cm^2 fluence with varying irradiance. Fluences greater than 10 J/cm^2 have previously been associated with decreased cell viability and DNA damage [37]. A dataset of cells laser-treated with an 810 nm wavelength stimulated at an intensity of 150 mW/cm^2 for 60 s was obtained from a previous study [33]. New treatments with the 1064 nm laser were applied at 300 mW/cm^2 for 30 s and 200 mW/cm^2 for 45 s. A continuous 1064 nm wavelength was used to test and establish the wavelength dependence in comparison to the previous 810 nm exposure experiments.

2.3. Fluorescence Imaging

All cells were seeded onto 35 mm glass-bottom dishes (Cellvis, Mountain View, CA, USA) for live cell imaging. Fluo-8 (Abcam, Boston, MA, USA) was used for fluorescence staining to monitor calcium activity. The dye was mixed with Hank's Balanced Salt Solution (HBSS) to a final concentration of 0.8 and 1.6 μM for βTC6 and αTC1, respectively, and incubated at 37 °C for 30 min. All cells were counterstained with NucBlue to assist with segmentation. Each plate was imaged at 5 s intervals for 2 min prior to treatment to obtain control data. Following photostimulation, the cells were then imaged for 2 min intervals at t = 5, 10, and 15 min to minimize photobleaching.

2.4. AI-Assisted Pipeline

BetaBuddy is a computer vision pipeline that provides a series of algorithms to automatically segment, register, and track the imaged cells over time, as shown in Figure 1. We recently provided a full description of the development and application of BetaBuddy [36]. Briefly, microscopic images acquired using an imaging system first undergo a file type conversion process to standard format (i.e., TIFF files). Next, the calcium-sensitive Fluo-8 intensity channel is merged with the DAPI channel (visualization of nuclei) so that individual cells may be better identified. The segmentation of the images is performed using Cellpose [35], a generalist algorithm designed for the successful segmentation of multiple different cell types.

To further assist with accurate segmentation, composite images containing the maximum intensity value of every pixel were produced so that cell boundaries could be more strictly defined during periods of low intensity. Due to the fact that β- and α-cells are typically found to be clustered and therefore do not move within the observation and image acquisition time (15 min), this process was justifiable, as spatial locations were not too significantly changed during fluorescence imaging. The composite images then underwent the segmentation process, and the resulting masks were overlayed with their respective image stacks. The Fiji plugin Trackmate [38] identifies the ROIs obtained from the mask

images and uses them to register the cells. Each cell is then tracked across every frame, providing individualized spatial and time-series data. Data obtained from the registration and tracking of the ROIs are output into a CSV file, which is then used to perform automated background subtraction and normalization. Once the data have been normalized, an automated calcium spike detection procedure is used to analyze and represent changes in calcium dynamics.

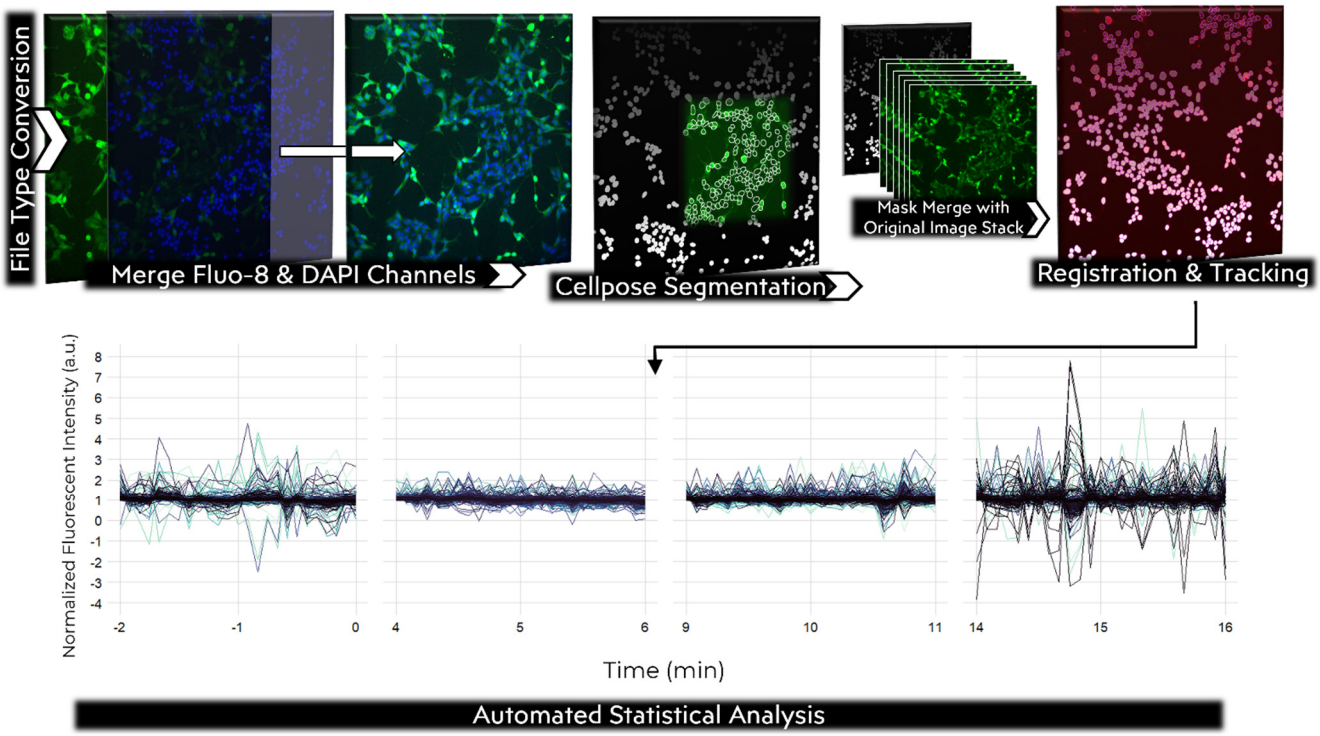

Figure 1. Modified BetaBuddy flowchart. The BetaBuddy pipeline automatically converts the fluorescence image files into a workable TIFF file type, merges the FITC (calcium fluorophore) and DAPI (nuclei) channels together, and performs a series of image processing steps to prepare the images for segmentation. A deep learning algorithm, Cellpose, is then utilized to segment the cells, and all designated ROIs are tracked and registered across each time frame using Fiji macro scripts. Automated statistical analysis is then performed on all registered cells using R language. Each line in the graph represents a registered cell over the designated image time. BetaBuddy's original script was modified to analyze the cells at each of the designated timepoints in the photobiomodulation experiment (t = 0, 5, 10, and 15 min). Cells were monitored in 2 min time windows at 5 s intervals.

2.5. Calcium Spike Detection

Automated calcium spike detection was performed separately for all timepoints of each trial. To maintain consistency with the original experiment, calcium spikes were defined by 10% increases in fluorescence intensity.

The automated algorithms provided an opportunity for more sophisticated normalization and background subtraction procedures. Therefore, a threshold based on a moving average, as reported in the previously published results [33], was no longer needed. Instead, the algorithm was used to locate all intensity peaks over time for each individual cell. Calcium spikes were then defined using two parameters: (1) an identified peak had an increase in fluorescence intensity $\geq$ 10% from its immediately preceding measured timepoint and/or (2) the net change between two identified peaks in activity was $\geq$10%. An example 2 min imaging period highlighting these spikes for each cell type is illustrated in Figure 2.

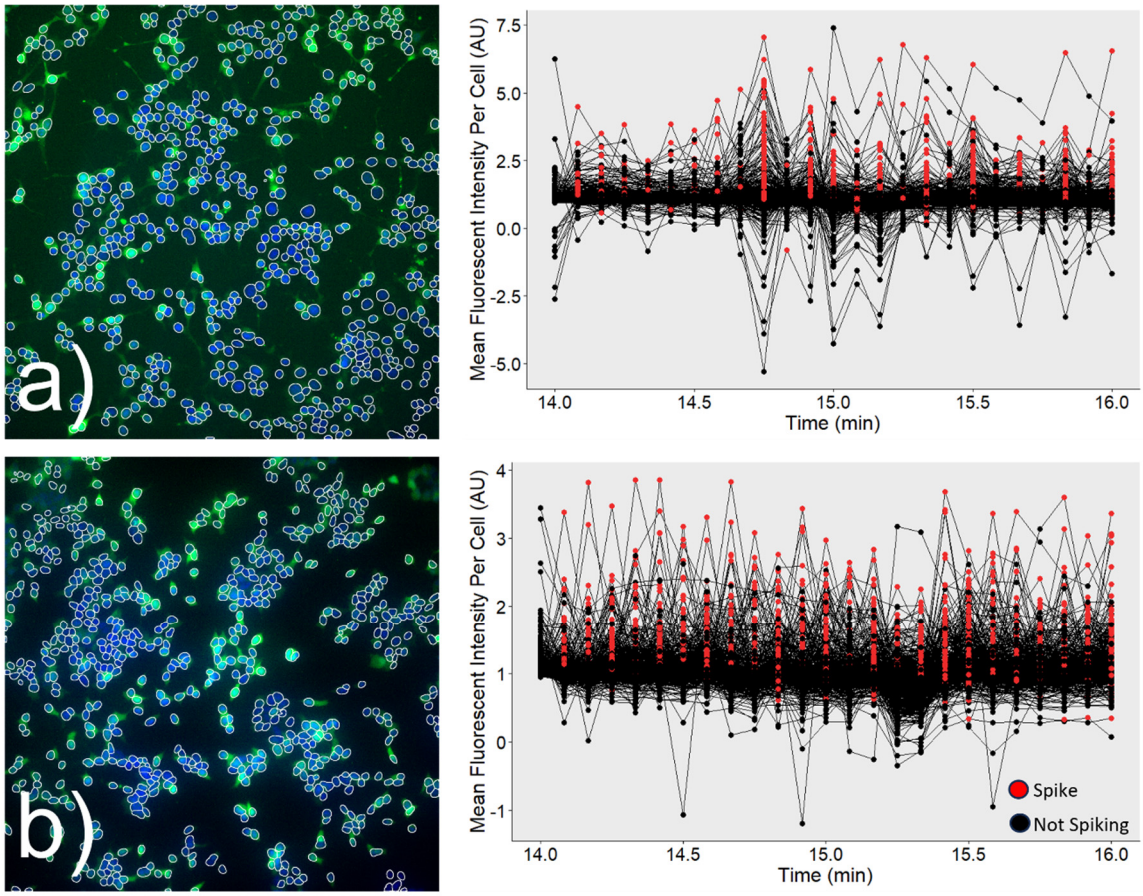

Figure 2. Calcium spike analysis. All cells were stained with Fluo-8 (green) to measure calcium intensity. Nucblue was used for nuclear staining (blue). Each registered ROI is outlined in white. Spikes in fluorescence intensity are automatically detected for each registered ROI. Spiking activity is calculated for each 2 min imaging period. A representative sample of calcium intensity fluctuations is shown at t = 15 min for one experiment set of α-cells (**a**) and another of β-cells (**b**). Two 2 min acquisitions of Fluo-8 images at 5 s intervals in multiple cells are shown, respectively. Red dots indicate a designated calcium spike.

2.6. Fold-Change Determination

The fold-change increases were calculated for each trial for both β- and α-cells. The activity at each timepoint was defined as the number of calcium spikes divided by the number of cells over time and normalized by the calcium spikes at t = 0 prior to stimulation. The fold-rise in calcium activity was averaged over all trials at each timepoint (t = 0, 5, 10, and 15 min).

3. Results

3.1. Dataset Reanalysis

Using BetaBuddy, more ROIs were identified with respect to the number of cells used in the original calculations. With manual segmentation, the identification of ROIs can be more challenging, biased, and exceedingly more time-consuming. Thus, a representative sample is often used to carry out reproducible calculations throughout all timepoints. With BetaBuddy, nearly every cell within each frame is registered for statistical calculation and could likely affect the overall results in changing fluorescence intensity patterns. To provide a quantitative comparison, the number of ROIs determined manually and by BetaBuddy was monitored for each experiment set. As shown in Figure 3, there was a significant difference in the number of ROIs determined between the manual and automated analyses.

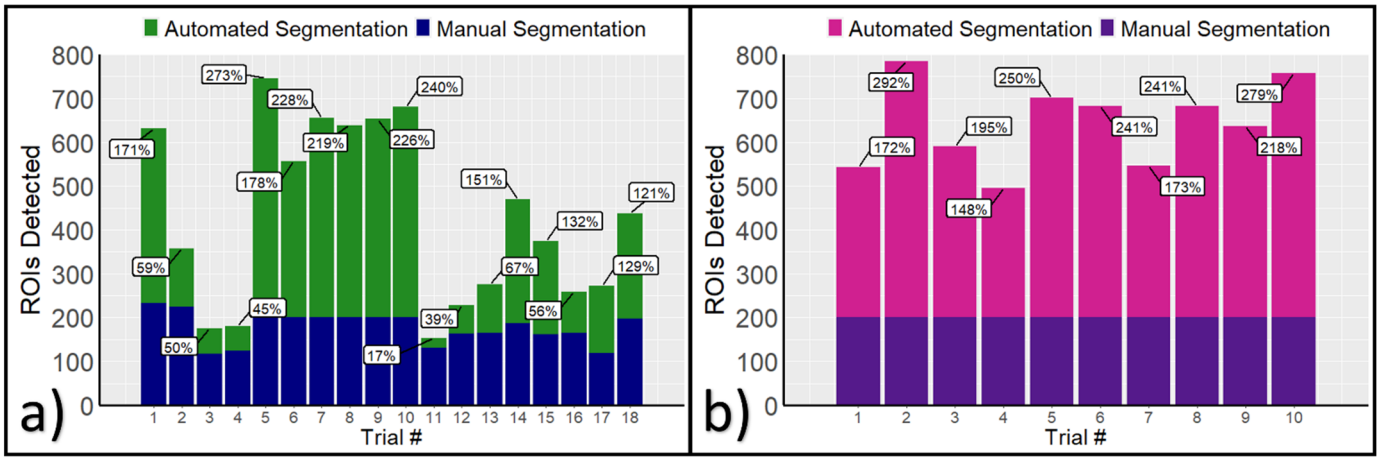

Figure 3. Improving ROI detection. (**a**) Average number of ROIs detected for all βTC6 experiments. Labels represent the percent change between the manual and automated analyses. (**b**) Average ROIs identified in αTC1 experiments with percent change.

The mean percent change between the number of ROIs analyzed between the two methods was 133% for the βTC6 cells and 221% for the αTC1 cells, which were fluorescently monitored and recorded in 18 or 10 independent experiments, respectively. This comparison provides convincing evidence that calcium dynamics in islet cells are more accurately represented by the computer vision machine learning pipeline.

The automated cell segmentation and statistical analysis of calcium dynamics determined significant increases in activity for both the βTC6 and αTC1 cells in response to PBM. The reanalyzed results were, in general, in agreement with the previously reported, manually analyzed results, but with subtle differences. The magnitude of increase in calcium spiking activity was previously reported as ~3-fold. Figure 4 shows the newly reanalyzed results using BetaBuddy, indicating that such increases were <~3-fold.

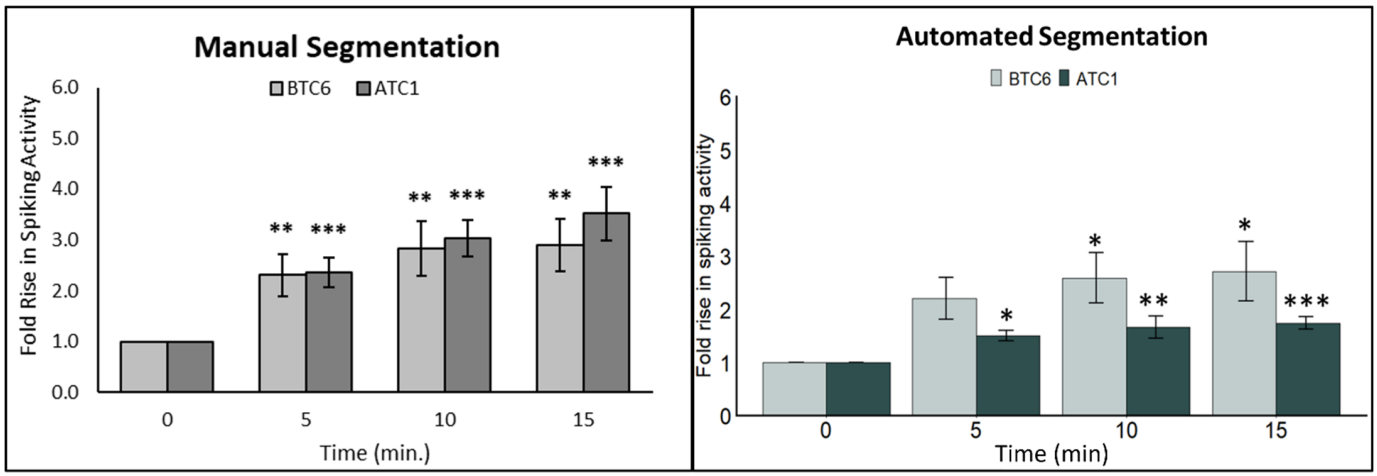

(**a**) (**b**)

Figure 4. Validation of results. Significant increases in calcium activity found in the original experiment (**a**) using manual analysis were generally confirmed by applying BetaBuddy (**b**). While the magnitude of increases appears to have been overestimated manually, the overall trend of PBM-induced calcium spiking in both cell types is validated, with a few subtle differences (see text). An ANOVA test was performed; * $p < 0.05$, ** $p < 0.01$, and *** $p < 0.001$.

The difference was subtle, and it reassured the investigators that hand-drawn cell segmentation and analysis were reasonable but likely to be less accurate and obviously more laborious. More interestingly, however, unlike the α-cells, the β-cells did not exhibit a

significant increase in calcium activity until after 10 min following the PBM treatment. This subtlety was not noticeable in the manual analysis. Moreover, the calcium activity in the α-cells increased within 5 min following PBM but did not further increase. This contrasts with the previous results, which showed that the calcium activity in the α-cells appeared to steadily increase over the 15 min observation time.

3.2. Wavelength Dependency

Further investigations were conducted following the original 810 nm experiments to obtain insights into cell-type-dependent responses to 1064 nm laser therapy. While maintaining the same fluence as in the original experiments (9 J/cm^2), cells were stimulated using the 1064 nm laser at 300 mW/cm^2 for 30 s and 200 mW/cm^2 for 45 s. The results are summarized and shown in Figure 5.

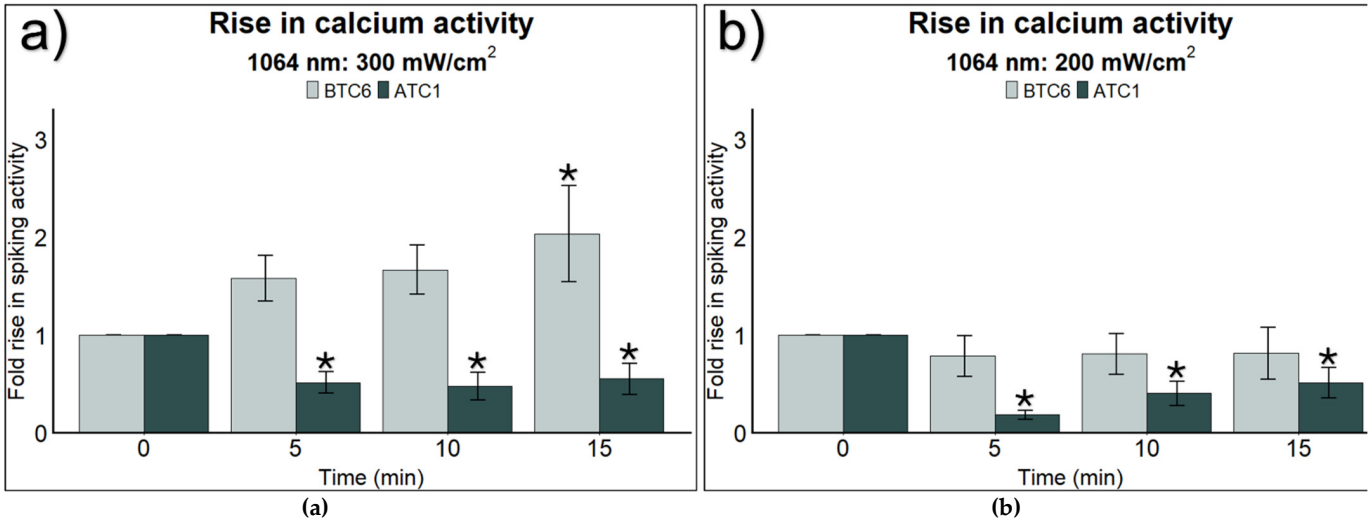

(a) **(b)**

Figure 5. Cell-type responses to 1064 nm PBM. (**a**) The application of the 1064 nm laser with a 300 mW/cm^2 intensity resulted in a significant increase in calcium activity in the β-cells at t = 15 min. Significant inhibition of calcium activity was present at all timepoints in the α-cells. (**b**) Applying a 200 mW/cm^2 intensity with the 1064 nm laser resulted in the inhibition of calcium activity when compared to the control for both cell types. The data represent the mean ± SEM of fold-rise in calcium spiking activity for the β- and α-cells from 12 and 9 independent experiments, respectively. Approximately 500 to 600 cells were segmented and analyzed in each experiment. * $p < 0.05$.

PBM significantly increased the calcium activity of the β-cells at the 15 min timepoint with the application of a 300 mW/cm^2 intensity. This finding is not totally inconsistent with the results we obtained using 810 nm (see Figure 4), although the fold-rise in calcium spiking activity decreased modestly. Interestingly, no significant increase was observed when the laser intensity was reduced to 200 mW/cm^2 but applied for a longer duration (e.g., 30 vs. 45 s) to maintain the same fluence (Figure 5a). The wavelength dependence was more pronounced in the α-cells. Neither of the two laser intensities we used were capable of increasing the calcium activity in this cell type. In fact, the PBM-induced calcium activities in the α-cells appeared to be inhibited when 1064 nm photostimulation was applied.

4. Discussion

The changes in calcium activity observed are consistent with our previous understanding of CCO absorption spectra. CCO absorbs strongly at ~800 nm [24,25], and thus more robust responses in calcium dynamics should be expected when carrying out stimulation with an 810 nm laser. At 1064 nm, its absorption coefficient is reduced by ~3-fold [27], which provides a simple explanation of the wavelength-dependent modulation of calcium

dynamics in islet cells. While the fluence was fixed at 9 J/cm^2, we varied the laser intensity and time duration to assess whether the islet cell physiology depends on the rate of photoenergy delivery. Consistent with a generally accepted paradigm in the literature, a stronger light intensity applied for a short time duration is more effective in inducing photostimulatory responses. It is interesting to note that our results may be indicative of a biphasic dose response. Multiple studies have demonstrated that changing the fluence resulted in an oscillation between stimulatory or inhibitory responses at varying wavelengths [39], and longer wavelengths tend to be more effective at lower doses [26,39]. Our findings partially confirm this trend at 1064 nm. However, a longer duration of treatment at a lower irradiance (e.g., 200 mW/cm^2) resulted in an inhibitory effect on calcium activity, especially when compared to the stimulatory effect observed at 300 mW/cm^2 in the β-cells.

The calcium dynamics studies we performed were monitored and recorded for 15 min following PBM stimulation. Therefore, we next assessed the PBM effects over a longer observation time period. In a set of proliferation studies, alamarBlue was used to evaluate the viability of β- and α-cells after 24 h in response to PBM therapy. Again, the fluence was fixed at 9 J/cm^2 for both 810 and 1064 nm photostimulation. For the β-cells, a single PBM treatment at 0 h increased the cell viability when using both the 810 nm and 1064 nm lasers. However, the application of the 810 nm laser demonstrated greater cell viability as compared to the control, unexposed cells (Figure 6). Again, this finding is in agreement with and can be explained by a higher absorption of CCO at 810 nm. In contrast, the same PBM treatment induced no statistically significant difference in α-cell viability. Such cell-type dependence is not readily understood, nor is it easily explained by differential absorption, and this reiterates the challenges of (1) having to optimize PBM for different cell types and (2) establishing generalized photocoupling mechanisms. To further compound this challenge, we chose to treat the cells with two PBM treatments at 0 and 6 h. These two treatments applied within 6 h of each other displayed an inhibitory effect on β-cells (Figure 6). This is reminiscent of the biphasic dose response that is well characterized in pharmacodynamics [39]. Interestingly, no PBM treatment was capable of increasing cell viability in the α-cells. The PBM treatment frequency may have to be optimized for different cell/tissue types, in addition to optimizing the PBM parameters, including the wavelength, fluence, and energy deposit rate.

The potential benefits of PBM therapy continue to be encouraging and are reinforced by new information that is being obtained through computational methods. Although we found that hand segmentation and manual analysis led to similar conclusions, automated methods are best for implementation in future experiments for multiple reasons. First, with machine learning techniques, we are able to segment and analyze more cells, thus increasing accuracy. Second, automated pipelines are faster and more efficient for batch analysis. The time requirement for one set of data is reduced from tens of hours over a few days to less than 15 min, and the results are no longer subject to human biases. Third, through automated methods, we have the capability to now explore cell–cell communication, including the cell feedback mechanisms of pancreatic cells through calcium signaling. Finally, as proposed below, these faster, more accurate results can provide a basis for formulating novel working models to determine photocoupling mechanisms that are likely cell-type-dependent, which further illustrates the utility of implementing a computer vision pipeline.

The development and application of the automated pipeline offer the capability to effortlessly determine the active population of cells. Consistent with our previous definition [33], any cell that spikes at least once within a given experiment was considered active. Because each cell was not only segmented but registered, tracking individual cells over the 15 min observation period was straightforward. As shown in Figure 7, we are

now able to monitor PBM effects using multiple independent samples and observe trends in the active populations. Again, this illustrates one of the advantages of using an automated pipeline over manual analysis. More in-depth analyses are underway to determine coupling mechanisms that might explain a plausible increase in the active cell populations.

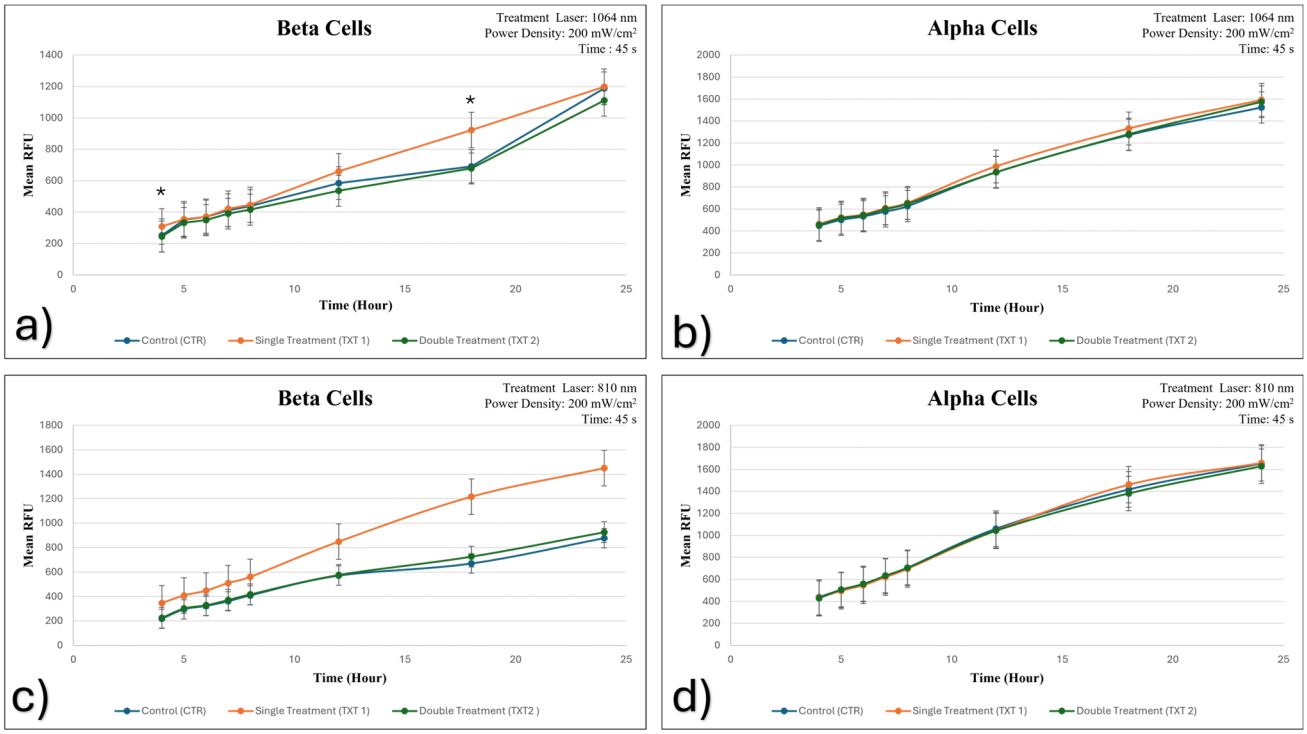

Figure 6. Biphasic Response of PBM on cell viability. β- and α-cells were treated with PBM, and fluorescence intensity was measured with an AlamarBlue assay over a 24 h period. Each experimental condition contained a control, a single initial PBM treatment, and a double PBM treatment at 0 and 6 h. The relative fluorescence intensity following the application of 1064 nm laser therapy was quantified for β-cells (**a**) and α-cells (**b**), respectively. The cell-type-dependent responses are also displayed post-treatment with an 810 nm laser (**c**,**d**). At both wavelengths, β-cells exhibited an increase in cell viability with a single PBM treatment, with a significant difference ($p < 0.05$) at t = 4 h and t = 8 h with the 1064 nm laser. Two treatments within 6 h appeared to negate such PBM-induced responses. No PBM treatment led to any significant difference in α-cells. The initial cell seeding density was 5×10^5 cells/well. The data represent the mean ± SEM of n = 4 independent experiments.

Trial-specific data can better highlight the cell-type-dependent response to PBM. New but physiologically significant results are now made possible because we implemented a computer vision pipeline that is proven to be capable of elucidating a subtle but important cell-type dependence when cells are treated with photostimulation. The two major cell types found in islet cell population are α- and β-cells. These two cell types are known to work to oppose one another. β-cells produce insulin to lower the blood glucose concentration, whereas α-cells respond to hypoglycemia and produce glucagon to signal the liver to release and elevate the glucose level. Two counteracting hormones are produced in these different cell types, but, nonetheless, they are found in close proximity to each other [40]. Recent mathematical modeling suggests that there could be a paracrine feedback mechanism through which glucagon produced by α-cells may produce a stimulatory effect on adjacent cells (e.g., β-cells) [41]. This feedback mechanism may involve paracrine or cell–cell communication, which is known to depend on calcium dynamics [42]. Based on the newly discovered results using the machine learning pipeline, a working model is proposed in Figure 8, in which external photostimulation affects more than one cell type in the islet.

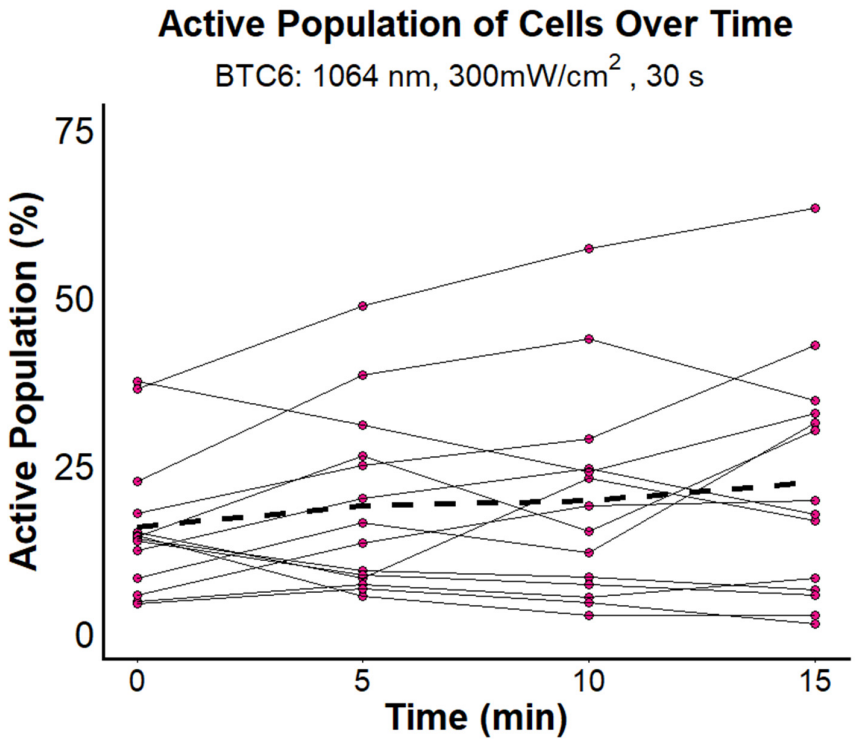

Figure 7. Effects of photobiomodulation on active cell population. Upon receiving PBM treatment, the percentage of active cells in the cell population tends to increase with respect to the pre-stimulation control. Shown in the figure is a representative sample of βTC6 cells with the application of 1064 nm laser therapy at a 300 mW laser power. The dashed line is the mean of all the trials (n = 14 with approximately 1×10^4 cells).

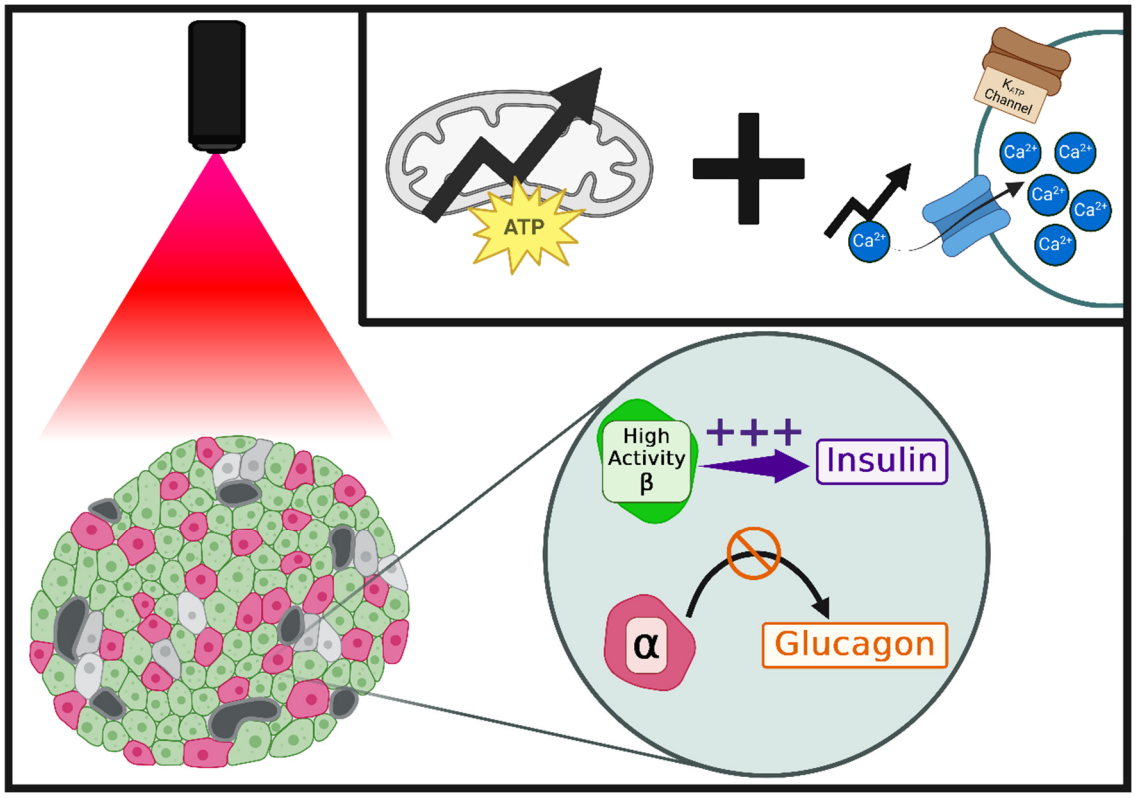

Figure 8. Working model [43]. PBM is not expected to directly activate calcium channels. Instead, the generation of ATP in the mitochondria facilitates the closure of K_{ATP} channels, initiating the entry of Ca^{2+} into the cell. This calcium influx triggers the release of insulin in β-cells to elevate blood glucose

levels. We postulate that stimulated β-cells in the active mode mediate such an insulin increase, thus lowering blood glucose levels. The role of PBM-induced calcium spiking in α-cells is less clear. Two competing hypotheses include a paracrine interaction between the two different cell types or an anti-correlation between enhanced calcium spiking and glucagon secretion. Since PBM-induced glucagon secretion was demonstrated to depend on the extracellular glucose concentration [33], a challenge remains to develop a more complex network of signaling mechanisms. While detailed cell-type-dependent photocoupling mechanisms are being further investigated, a computer vision-based automated pipeline has demonstrated its potential to discover novel islet physiology that may lead to the optimization of a non-biological therapeutic approach to pre-treating isolated islets prior to transplantation to type I diabetic patients.

Since the amount of insulin secretion has been shown to increase with enhanced calcium spiking [33], the active β-cell population is presumed to respond to PBM and increase insulin secretion. In contrast, α-cells behave differently, and elevated calcium spiking in glucagon-secreting cells likely produces different effects. Unlike β-cells, α-cells are electrically active even in the absence of glucose [44]. However, both α- and β-cells possess ATP-sensitive potassium channels (K_{ATP}) that regulate calcium channels and the subsequent release of metabolic hormones from islet cells. This highlights an islet physiology conundrum in that the same channels appear to operate in a cell-type-dependent manner. Two competing hypotheses are testable. First, calcium spiking in α-cells is independent of K_{ATP} channels. This hypothesis can be validated by measuring the ATP level in α-cells in response to PBM. Second, alternatively, or perhaps more interestingly, calcium spiking in α-cells exhibits an anti-correlation with glucagon secretion. While this alternative hypothesis is consistent with the established feedback mechanism between insulin and glucagon for the regulation of glucose homeostasis, such a potential negative feedback mechanism may also depend on the extracellular glucose environment [44], as well as cell-to-cell communication through calcium spiking between adjacent cells. It should be noted here that there are other potential mechanisms that warrant more studies. For example, light-sensitive molecules (e.g., ion channels) that are preferentially expressed in different cell types can indeed respond to PBM in different manners, but they remain speculative and not fully understood.

The complexity of glucose homeostasis is yet to be fully elucidated, but such interpretation is beyond the scope of this paper. However, it should be re-emphasized that the computer vision algorithms are capable of generating interesting and unexpected results that could otherwise be overlooked. We have demonstrated the successful implementation of a computer vision pipeline that led us to perform in-depth analyses of a large body of existing cell images without having to revert to tedious manual methods. In addition, we applied the same pipeline to newly acquired data to examine wavelength dependence and further illuminate a potential photocoupling mechanism(s). Finally, the application of photostimulation to a whole islet is underway to validate the utility of phototherapy for improving the viability and functionality of isolated islet cells prior to clinical transplantation.

5. Conclusions

While manual segmentation methods have been proven to be acceptable, automated analysis appears to be the most viable option for future work. Computer vision pipelines are faster and more efficient for batch analysis of large datasets. Furthermore, automated methods are able to identify and segment more cells within individual images and can register each cell for detailed analyses that could lead to the potential discovery of the physiology of islet cells.

Using these new methods, we were able to identify substantially more cells than in the previous analysis and monitor changes on a cell-by-cell basis. From this analysis, we can

conclude that the findings from the original experiment using manual segmentation were generally validated, and the application of photobiomodulation significantly increases calcium activity in both βTC6 and αTC1 cells. However, these stimulatory effects are modulated by a biphasic dose response and necessitate optimal parameters for PBM application. This has significant implications for precision medicine in the future, as it suggests that, in addition to existing variables, including wavelength, fluence, mode, and exposure rate, and dose–response relationships, cell-type dependence must also be considered when refining parameters for these therapies. Consequently, future studies should account for such variables in their analyses. Moreover, there are a multitude of other NIR wavelengths that have been used for PBM therapies, including studies for diabetes mellitus. These wavelengths range from ~660 nm to 980 nm [21,26]. Our current studies can provide a rapid and accurate experimental and analytical platform to further explore and validate wavelength dependence. The subtle but important differences in the apparent cell-type-dependent calcium dynamics may lead to the optimization of photostimulation so that it specifically targets whole islets and regulates the insulin secretion feedback mechanisms. Future work will include the application of image processing algorithms using intact whole islets. The targeted analysis of complex biosystems with improved accuracy is expected to lead to a better characterization of viable islets. This step highlights the utility of automated segmentation and analysis for islet transplantation in patients with type I diabetes.

Author Contributions: Conceptualization, K.F.; methodology, K.F. and A.M.A.; software, K.F. and A.M.A.; validation, K.F. and A.M.A.; formal analysis, K.F. and A.K.; investigation, K.F. and A.K.; resources, C.M.D., J.M.L. and M.C.L.; data curation, K.F.; writing—original draft preparation, K.F.; writing—review and editing, M.C.; visualization, K.F. and M.C.; supervision, M.C.; project administration, M.C.; funding acquisition, J.M.L. and M.C. All authors have read and agreed to the published version of the manuscript.

Funding: This work was supported by the NIH Predoctoral Training Grant (HL134613; PI, Kytai Nguyen), the University of Texas System Rising STARs Award (J.M.L.), the CPRIT First Time Faculty Award (J.M.L.), and the Alfred R. and Janet H. Potvin Endowment (M.C.).

Institutional Review Board Statement: Not applicable.

Informed Consent Statement: Not applicable.

Data Availability Statement: The datasets used in this study are available upon request from the author. The source code used for analysis is openly available and can be found in the following GitHub repository: https://github.com/jacobluber/BetaBuddy.

Acknowledgments: We would like to thank Caleb Liebman for his invaluable contribution culturing mouse insulinoma cells and producing a series of calcium images used in this study.

Conflicts of Interest: The authors declare no conflicts of interest.

References

1. Hamblin, M.R. Mechanisms and Mitochondrial Redox Signaling in Photobiomodulation. *Photochem. Photobiol.* **2018**, *94*, 199–212. [CrossRef] [PubMed]
2. Wang, X.; Tian, F.; Soni, S.S.; Gonzalez-Lima, F.; Liu, H. Interplay between up-regulation of cytochrome-c-oxidase and hemoglobin oxygenation induced by near-infrared laser. *Sci. Rep.* **2016**, *6*, 30540. [CrossRef] [PubMed]
3. Castro, K.M.R.; de Paiva Carvalho, R.L.; Junior, G.M.R.; Tavares, B.A.; Simionato, L.H.; Bortoluci, C.H.F.; Soto, C.A.T.; Ferraresi, C. Can photobiomodulation therapy (PBMT) control blood glucose levels and alter muscle glycogen synthesis? *J. Photochem. Photobiol. B* **2020**, *207*, 111877. [CrossRef] [PubMed]
4. de Freitas, L.F.; Hamblin, M.R. Proposed Mechanisms of Photobiomodulation or Low-Level Light Therapy. *IEEE J. Sel. Top. Quantum Electron. Publ. IEEE Lasers Electro Opt. Soc.* **2016**, *22*, 7000417. [CrossRef]
5. Deana, N.F.; Zaror, C.; del Sol, M.; Bagnato, V.S.; Alves, N. Wound contraction rate in excised and unexcised burn wounds with laser photobiomodulation: Systematic review and meta-analysis of preclinical studies. *Burns* **2023**, *49*, 261–274. [CrossRef]

6. Mosca, R.C.; Ong, A.A.; Albasha, O.; Bass, K.; Arany, P. Photobiomodulation Therapy for Wound Care: A Potent, Noninvasive, Photoceutical Approach. *Adv. Skin Wound Care* **2019**, *32*, 157–167. [CrossRef]
7. Ocon, C.A.; dos Santos, S.A.; Caires, J.R.; de Oliveira, M.F.D.; Serra, A.J.; Leal-Junior, E.C.; de Carvalho, P.d.T.C. Effects and parameters of the photobiomodulation in experimental models of third-degree burn: Systematic review. *Lasers Med. Sci.* **2019**, *34*, 637–648. [CrossRef]
8. Begum, R.; Powner, M.B.; Hudson, N.; Hogg, C.; Jeffery, G. Treatment with 670 nm Light Up Regulates Cytochrome C Oxidase Expression and Reduces Inflammation in an Age-Related Macular Degeneration Model. *PLoS ONE* **2013**, *8*, e57828. [CrossRef]
9. Hamblin, M.R. Photobiomodulation for Alzheimer's Disease: Has the Light Dawned? *Photonics* **2019**, *6*, 77. [CrossRef]
10. Yang, L.; Wu, C.; Parker, E.; Li, Y.; Dong, Y.; Tucker, L.; Brann, D.W.; Lin, H.W.; Zhang, Q. Non-invasive photobiomodulation treatment in an Alzheimer Disease-like transgenic rat model. *Theranostics* **2022**, *12*, 2205–2231. [CrossRef]
11. das Neves, M.F.; Aleixo, D.C.; Mendes, I.S.; Lima, F.P.S.; Nicolau, R.A.; Arisawa, E.A.L.; Lopes-Martins, R.A.B.; Lima, M.O. Long-term analyses of spastic muscle behavior in chronic poststroke patients after near-infrared low-level laser therapy (808 nm): A double-blinded placebo-controlled clinical trial. *Lasers Med. Sci.* **2020**, *35*, 1459–1467. [CrossRef] [PubMed]
12. Lampl, Y.; Zivin, J.A.; Fisher, M.; Lew, R.; Welin, L.; Dahlof, B.; Borenstein, P.; Andersson, B.; Perez, J.; Caparo, C.; et al. Infrared laser therapy for ischemic stroke: A new treatment strategy: Results of the NeuroThera Effectiveness and Safety Trial-1 (NEST-1). *Stroke* **2007**, *38*, 1843–1849. [CrossRef] [PubMed]
13. Yang, M.; Yang, Z.; Wang, P.; Sun, Z. Current application and future directions of photobiomodulation in central nervous diseases. *Neural Regen. Res.* **2020**, *16*, 1177–1185. [CrossRef]
14. Dompe, C.; Moncrieff, L.; Matys, J.; Grzech-Leśniak, K.; Kocherova, I.; Bryja, A.; Bruska, M.; Dominiak, M.; Mozdziak, P.; Skiba, T.H.I.; et al. Photobiomodulation—Underlying Mechanism and Clinical Applications. *J. Clin. Med.* **2020**, *9*, 1724. [CrossRef]
15. Van Tran, V.; Chae, M.; Moon, J.-Y.; Lee, Y.-C. Light emitting diodes technology-based photobiomodulation therapy (PBMT) for dermatology and aesthetics: Recent applications, challenges, and perspectives. *Opt. Laser Technol.* **2021**, *135*, 106698. [CrossRef]
16. Glass, G.E. Photobiomodulation: The Clinical Applications of Low-Level Light Therapy. *Aesthet. Surg. J.* **2021**, *41*, 723–738. [CrossRef]
17. McColloch, A.; Liebman, C.; Liu, H.; Cho, M. Alterted Adipogenesis of Human Mesenchymal Stem Cells by Photobiomodulation Using 1064 nm Laser Light. *Lasers Surg. Med.* **2021**, *53*, 263–274. [CrossRef]
18. McColloch, A.; Liu, H.; Cho, M. Reversal of stem cell-derived hypertrophic adipocytes mediated by photobiomodulation (1064 nm). *Transl. Biophotonics* **2021**, *3*, e202100006. [CrossRef]
19. Silva, G.; Ferraresi, C.; de Almeida, R.T.; Motta, M.L.; Paixão, T.; Ottone, V.O.; Fonseca, I.A.; Oliveira, M.X.; Rocha-Vieira, E.; Dias-Peixoto, M.F.; et al. Infrared photobiomodulation (PBM) therapy improves glucose metabolism and intracellular insulin pathway in adipose tissue of high-fat fed mice. *Lasers Med. Sci.* **2018**, *33*, 559–571. [CrossRef]
20. Bonifacio, M.; Benfato, I.D.; de Almeida Cruz, M.; de Sales, D.C.; Pandolfo, I.L.; Quintana, H.T.; Carvalho, C.P.F.; de Oliveira, C.A.M.; Renno, A.C.M. Effects of photobiomodulation on glucose homeostasis and morphometric parameters in pancreatic islets of diabetic mice. *Lasers Med. Sci.* **2022**, *37*, 1799–1809. [CrossRef]
21. Oyebode, O.; Houreld, N.N.; Abrahamse, H. Photobiomodulation in diabetic wound healing: A review of red and near-infrared wavelength applications. *Cell Biochem. Funct.* **2021**, *39*, 596–612. [CrossRef] [PubMed]
22. de Sousa, R.G.; Batista, K.d.N.M. Laser therapy in wound healing associated with diabetes mellitus—Review. *An. Bras. Dermatol.* **2016**, *91*, 489–493. [CrossRef] [PubMed]
23. Magri, A.M.P.; Fernandes, K.R.; Assis, L.; Mendes, N.A.; da Silva Santos, A.L.Y.; de Oliveira Dantas, E.; Rennó, A.C. Photobiomodulation and bone healing in diabetic rats: Evaluation of bone response using a tibial defect experimental model. *Lasers Med. Sci.* **2015**, *30*, 1949–1957. [CrossRef] [PubMed]
24. Wang, X.; Tian, F.; Reddy, D.D.; Nalawade, S.S.; Barrett, D.W.; Gonzalez-Lima, F.; Liu, H. Up-regulation of cerebral cytochrome-c-oxidase and hemodynamics by transcranial infrared laser stimulation: A broadband near-infrared spectroscopy study. *J. Cereb. Blood Flow Metab.* **2017**, *37*, 3789–3802. [CrossRef]
25. Kolyva, C.; Tachtsidis, I.; Ghosh, A.; Moroz, T.; Cooper, C.E.; Smith, M.; Elwell, C.E. Systematic investigation of changes in oxidized cerebral cytochrome c oxidase concentration during frontal lobe activation in healthy adults. *Biomed. Opt. Express* **2012**, *3*, 2550–2566. [CrossRef]
26. Wang, Y.; Huang, Y.-Y.; Wang, Y.; Lyu, P.; Hamblin, M.R. Photobiomodulation of human adipose-derived stem cells using 810nm and 980nm lasers operates via different mechanisms of action. *Biochim. Biophys. Acta* **2017**, *1861*, 441–449. [CrossRef]
27. Scholkmann, F.; Kleiser, S.; Metz, A.J.; Zimmermann, R.; Mata Pavia, J.; Wolf, U.; Wolf, M. A review on continuous wave functional near-infrared spectroscopy and imaging instrumentation and methodology. *NeuroImage* **2014**, *85*, 6–27. [CrossRef]
28. Aquino, A.E.; Sene-Fiorese, M.; Castro, C.A.; Duarte, F.O.; Oishi, J.C.; Santos, G.C.; Silva, K.A.; Fabrizzi, F.; Moraes, G.; Matheus, S.M.M.; et al. Can low-level laser therapy when associated to exercise decrease adipocyte area? *J. Photochem. Photobiol. B* **2015**, *149*, 21–26. [CrossRef]

29. Haythorne, E.; Rohm, M.; van de Bunt, M.; Brereton, M.F.; Tarasov, A.I.; Blacker, T.S.; Sachse, G.; Silva dos Santos, M.; Terron Exposito, R.; Davis, S.; et al. Diabetes causes marked inhibition of mitochondrial metabolism in pancreatic β-cells. *Nat. Commun.* **2019**, *10*, 2474. [CrossRef]
30. Müller, M.; Walkling, J.; Seemann, N.; Rustenbeck, I. The Dynamics of Calcium Signaling in Beta Cells—A Discussion on the Comparison of Experimental and Modelling Data. *Int. J. Mol. Sci.* **2023**, *24*, 3206. [CrossRef]
31. Gilon, P.; Chae, H.-Y.; Rutter, G.A.; Ravier, M.A. Calcium signaling in pancreatic β-cells in health and in Type 2 diabetes. *Cell Calcium* **2014**, *56*, 340–361. [CrossRef] [PubMed]
32. Liebman, C.; Vu, T.-M.; Phillips, A.; Chen, B.; Cho, M. Altered β-cell calcium dynamics via electric field exposure. *Ann. Biomed. Eng.* **2021**, *49*, 106–114. [CrossRef] [PubMed]
33. Liebman, C.; Loya, S.; Lawrence, M.; Bashoo, N.; Cho, M. Stimulatory responses in α- and β-cells by near-infrared (810 nm) photobiomodulation. *J. Biophotonics* **2022**, *15*, e202100257. [CrossRef]
34. Arena, E.T.; Rueden, C.T.; Hiner, M.C.; Wang, S.; Yuan, M.; Eliceiri, K.W. Quantitating the cell: Turning images into numbers with ImageJ. *WIREs Dev. Biol.* **2017**, *6*, e260. [CrossRef]
35. Rizwan, I.; Haque, I.; Neubert, J. Deep learning approaches to biomedical image segmentation. *Inform. Med. Unlocked* **2020**, *18*, 100297. [CrossRef]
36. Alsup, A.M.; Fowlds, K.; Cho, M.; Luber, J.M. BetaBuddy: An automated end-to-end computer vision pipeline for analysis of calcium fluorescence dynamics in β-cells. *PLoS ONE* **2024**, *19*, e0299549. [CrossRef]
37. Hawkins, D.H.; Abrahamse, H. The role of laser fluence in cell viability, proliferation, and membrane integrity of wounded human skin fibroblasts following helium-neon laser irradiation. *Lasers Surg. Med.* **2006**, *38*, 74–83. [CrossRef]
38. Schindelin, J.; Arganda-carreras, I.; Frise, E.; Kaynig, V.; Longair, M.; Pietzsch, T.; Preibisch, S.; Rueden, C.; Saalfeld, S.; Schmid, B.; et al. Fiji: An open-source platform for biological-image analysis. *Nat. Methods* **2012**, *9*, 676–682. [CrossRef]
39. Huang, Y.-Y.; Chen, A.C.-H.; Carroll, J.D.; Hamblin, M.R. Biphasic Dose Response in Low Level Light Therapy. *Dose-Response* **2009**, *7*, dose-response.09-027.Hamblin. [CrossRef]
40. Bosco, D.; Armanet, M.; Morel, P.; Niclauss, N.; Sgroi, A.; Muller, Y.D.; Giovannoni, L.; Parnaud, G.; Berney, T. Unique Arrangement of α- and β-Cells in Human Islets of Langerhans. *Diabetes* **2010**, *59*, 1202–1210. [CrossRef]
41. Rodriguez-Diaz, R.; Tamayo, A.; Hara, M.; Caicedo, A. The Local Paracrine Actions of the Pancreatic α-Cell. *Diabetes* **2019**, *69*, 550–558. [CrossRef] [PubMed]
42. Holter, M.M.; Saikia, M.; Cummings, B.P. Alpha-cell paracrine signaling in the regulation of beta-cell insulin secretion. *Front. Endocrinol.* **2022**, *13*, 934775. [CrossRef] [PubMed]
43. Fowlds, K. Created in BioRender [Internet]. 2025. Available online: https://biorender.com/s45z307 (accessed on 18 December 2024).
44. Le Marchand, S.J.; Piston, D.W. Glucose Decouples Intracellular Ca^{2+} Activity from Glucagon Secretion in Mouse Pancreatic Islet Alpha-Cells. *PLoS ONE* **2012**, *7*, e47084. [CrossRef] [PubMed]